

Towards Physically-Realizable Adversarial Attacks in Embodied Vision Navigation

Meng Chen¹, Jiawei Tu¹, Chao Qi², Yonghao Dang¹, Feng Zhou¹, Wei Wei¹, Jianqin Yin^{1,*}

Abstract—The deployment of embodied navigation agents in safety-critical environments raises concerns about their vulnerability to adversarial attacks on deep neural networks. However, current attack methods often lack practicality due to challenges in transitioning from the digital to the physical world, while existing physical attacks for object detection fail to achieve both multi-view effectiveness and naturalness. To address this, we propose a practical attack method for embodied navigation by attaching adversarial patches with learnable textures and opacity to objects. Specifically, to ensure effectiveness across varying viewpoints, we employ a multi-view optimization strategy based on object-aware sampling, which uses feedback from the navigation model to optimize the patch’s texture. To make the patch inconspicuous to human observers, we introduce a two-stage opacity optimization mechanism, where opacity is refined after texture optimization. Experimental results show our adversarial patches reduce navigation success rates by about 40%, outperforming previous methods in practicality, effectiveness, and naturalness. Code is available at: <https://github.com/chen37058/Physical-Attacks-in-Embodied-Navigation>.

I. INTRODUCTION

Embodied navigation [14], [15], [16], [17], [18] involves an agent navigating to an object or a specific position in an unseen environment. It is widely utilized in safety-critical scenarios, such as assisting individuals with disabilities in locating objects within their homes. When integrated with Deep Neural Networks (DNNs), embodied navigation agents leverage vision-based signal processing and sequential decision-making techniques [19], [20], [21], [22], leading to significant advancements. However, it is well-established that DNNs are vulnerable to adversarial examples [23], [24], [25], posing substantial risks to the real-world deployment of DNN-based embodied navigation agents.

Recently, research on adversarial attacks targeting embodied navigation agents has been limited. For instance, as shown in Fig.1 (a), [1] applied universal perturbations to the agent’s first-person observations, while in Fig.1 (b), [2] explored 3D adversarial camouflage by perturbing object textures in navigation scenes. Similar full-coverage texture attacks targeting object detectors have also been studied in [26], [27], [28], [29], [30]. However, these methods face practical challenges: affixing stickers to a camera is impractical, as attackers typically lack control over the agent’s camera, and altering the textures and shapes of scene objects

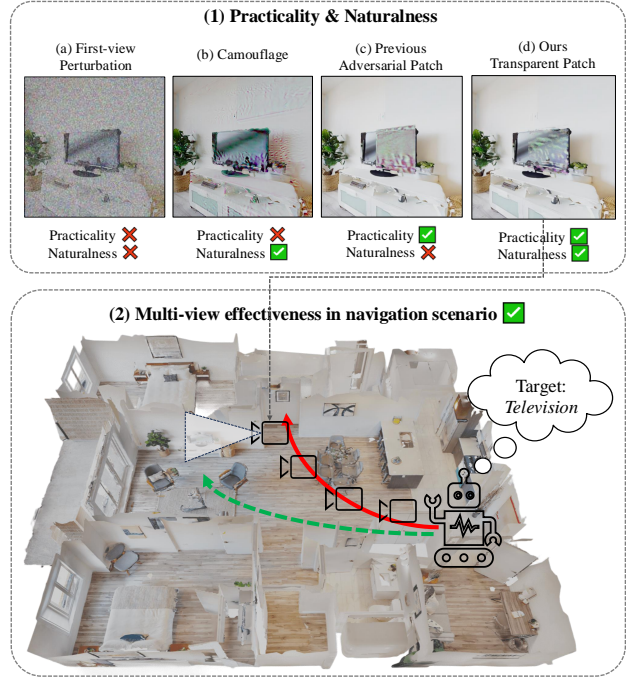


Fig. 1. **Motivation.** Previous attacks were either impractical or failed to achieve both naturalness and multi-view effectiveness in navigation tasks: (a) [1] applied universal perturbations to the agent’s first-person view. (b) [2] used camouflage techniques by perturbing the textures of 3D objects. (c) Earlier physical patch attacks [3], [4], [5], [6], [7], [8], [9], [10], [11], [12], [13] were more suited to clothing and lacked naturalness when applied to objects in navigation tasks. (d) Our adversarial patch, with learnable textures and opacity, is more natural and inconspicuous to human observers. The lower panel illustrates multi-view effectiveness in embodied navigation: applying the patch to the target TV prevents the agent from detecting the target across different viewpoints, leading to navigation failure (red path).

is costly, often requiring 3D printing, object replacement, or texture projection with projectors.

Some physically realizable adversarial patch attacks, as depicted in Fig.1 (c), [3], [4], [5], [6], [7], [8], [9], [10], [11], are widely used in areas such as traffic sign detection [4], [31] and facial recognition [32], [5], typically relying on techniques like Expectation over Transformation (EoT) [33], [34] to simulate real-world transformations, such as scaling and rotation. However, these methods are inadequate for the complex viewpoint changes in navigation scenarios. While multi-view adversarial patches [12], [13] are specifically designed to handle viewpoint variations, they are mainly suited for clothing and are unsuitable for objects in navigation scenes due to their low naturalness, making them easily noticeable by humans. **In summary, existing**

¹School of Artificial Intelligence, Beijing University of Posts and Telecommunications, Beijing 100876, China.

²Standard and Metrology Research Institute, China Academy of Railway Sciences Corporation Limited, Beijing 100081, China.

*Corresponding author.

e-mail: chenmeng@bupt.edu.cn.

physical attack methods fail to simultaneously meet two key criteria in navigation tasks: (1) Effectiveness under complex viewpoint variations; (2) Insufficient naturalness when attached to objects, making them easy to detect and defend against.

To develop a physically practical attack method that meets the dual requirements of multi-view effectiveness and naturalness in embodied navigation scenarios, as depicted in Fig.1 (d), we propose a novel approach involving the attachment of an adversarial patch with learnable textures and opacity to navigation target objects. **First, to address the challenge of multi-view effectiveness**, we employ a multi-view optimization strategy based on object-aware sampling to refine the adversarial patch. This process selects the most valuable viewpoints based on feedback from the navigation vision model. Using a physics-based differentiable renderer, we generate first-person images from these viewpoints, which are then fed into the navigation model to compute detection loss. We then use gradients to optimize both the patch’s texture and opacity. The multi-view effectiveness of our patch is shown in Fig.1 (lower panel). **Second, to improve the patch’s naturalness**, we incorporate an opacity optimization mechanism. The adversarial patch consists of a base texture with three RGB color channels and a single-channel opacity mask, both refined through multi-view optimization, ensuring adjustable transparency and rendering the patch inconspicuous to human observers.

We conducted experiments on the fundamental embodied navigation task, ObjectNav, using the HM3D scene datasets and compared our method against prior attack approaches, including those generating full-coverage textures for 3D objects and previously developed 2D pixel adversarial patches. The results demonstrate that our adversarial patches reduce navigation success rates by up to 40%. In addition to physical feasibility, our studies confirm the following key insight: (1) Multi-view optimization based on object-aware sampling is essential for ensuring the adversarial patch remains effective across all critical viewpoints. (2) Increasing the patch’s opacity preserves the same level of attack effectiveness while making it less noticeable to the human eye.

The contributions of this research are as follows:

- We propose a physically practical attack method for embodied vision navigation by attaching adversarial patches with learnable textures and opacity to objects.
- We introduce a multi-view optimization strategy based on object-aware sampling to enhance the patch’s multi-view effectiveness and incorporate opacity optimization to ensure the patch remains inconspicuous to human observers.
- Experimental results show that our adversarial patches reduce navigation success rates by approximately 40%, outperforming previous methods in practicality, effectiveness, and naturalness.

II. RELATED WORK

We briefly review related work on embodied navigation and physical adversarial attacks.

Embodied Navigation. Embodied navigation [18], [14], [19] refers to tasks where agents navigate the physical world using visual sensory inputs. Key tasks include object goal navigation [35], [36], [15], image goal navigation [37], [38], [39], visual language navigation [40], [41], [42], and embodied question answering [43]. Object goal navigation focuses on locating specific object categories (e.g., “bathroom”) in unknown environments, testing scene understanding and long-term memory. This foundational task has practical applications, such as assisting individuals with disabilities in finding objects. We focus on adversarial attacks in this task, critical for embodied AI and relevant to other tasks like visual language navigation and embodied question answering.

Physical Adversarial Attacks. Early work on adversarial attacks targeting embodied agents [2] focused on altering object properties (e.g., 3D shape, texture) in key scene views. Universal perturbations [1] explored patch applications on sensors but were impractical for real-world deployment. Adversarial patch attacks [3], [4], [5], [6], [7], [8], [9], [10], [11], widely applied in areas such as traffic sign detection [4], [31] and facial recognition [32], [5], modify the patches’ 2D pixel spaces without altering the original object, but they are limited by viewpoint changes in complex navigation scenarios. While multi-view adversarial patches [12], [13] are mainly suited for clothing and unsuitable for objects in navigation scenes because of their low naturalness, making them noticeable to humans. Our work aims to generate physically realizable adversarial examples for embodied navigation that simultaneously meet both multi-view effectiveness and naturalness in navigation tasks.

III. METHODOLOGY

A. Overview

In this section, we detail the proposed method for generating transparent adversarial patches, as illustrated in Fig. 2. (1) To improve the patch’s naturalness, we design the adversarial patch to consist of a base texture with three RGB color channels and a single-channel opacity mask, both refined through multi-view optimization, as detailed in Sec. III-E, ensuring adjustable transparency and rendering the patch inconspicuous to human observers. The transparent adversarial patch \mathcal{P}^{adv} with initialized random parameters is attached to the scene S on the target object. (2) To address the challenge of multi-view effectiveness, we employ a multi-view optimization strategy based on object-aware sampling to refine the adversarial patch. We first perform object-aware sampling: initialize camera viewpoints in batches and filter out configurations based on the navigation perception model f , yielding a viewpoint distribution V valuable for optimizing the patch, as detailed in Sec. III-C. (3) We apply this viewpoint distribution V for multi-view optimization to refine the adversarial patch, utilizing a differentiable renderer \mathcal{R} to render first-person images, which are then input into the navigation model f to compute the total detection loss. Gradients are leveraged to optimize the patch’s texture and opacity using PGD, as detailed in Sec. III-D.

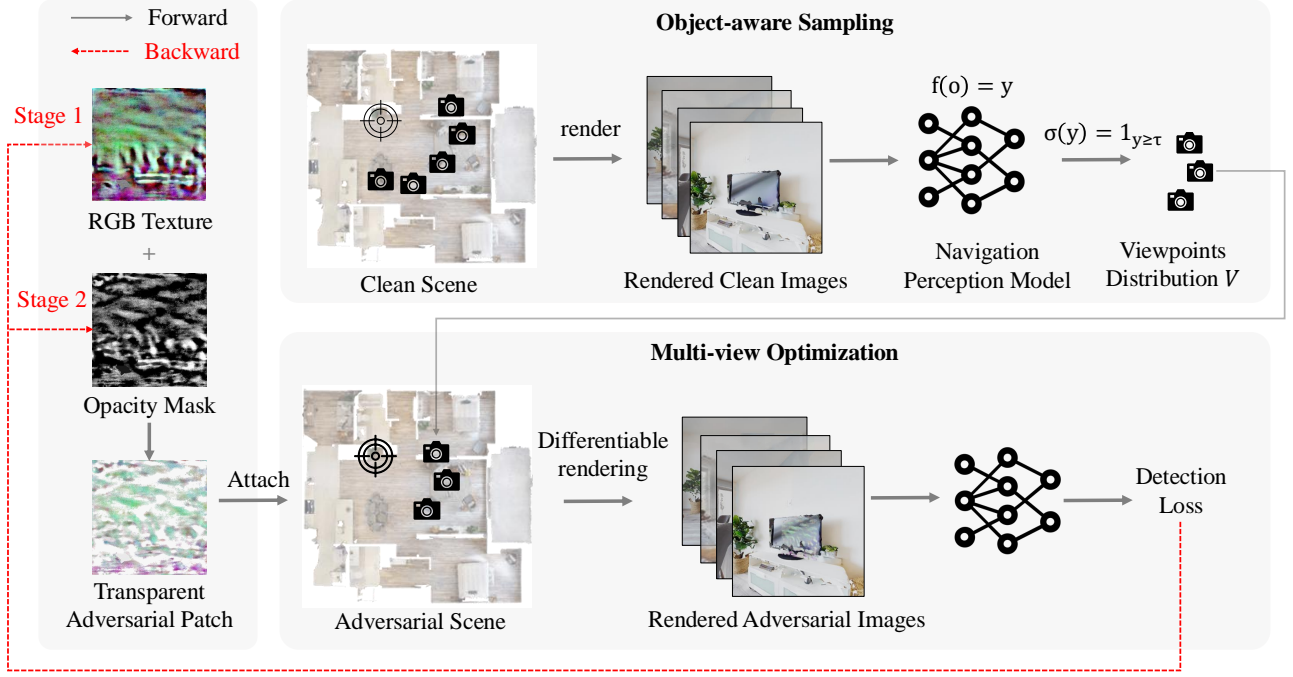


Fig. 2. Overview of our method for generating adversarial patches with learnable textures and opacity. (1) To improve naturalness, the patch is designed with a base texture (three RGB channels) and a single-channel **opacity mask**, both refined via multi-view optimization for adjustable transparency, making it inconspicuous to human observers. The initialized patch \mathcal{P}^{adv} is attached to the target object in scene \mathcal{S} . (2) For multi-view effectiveness, we use **object-aware sampling** to initialize camera viewpoints and filter them based on feedback from the navigation model f , yielding a valuable viewpoint distribution V . (3) We apply V in **multi-view optimization**, using a differentiable renderer \mathcal{R} to generate first-person images, which are fed into the navigation model f to compute detection loss. Gradients optimize the patch’s texture and opacity using PGD.

B. Problem Formulation

Given a scenario \mathcal{S} and a navigation perception model $f : o \rightarrow y$, our objective is to generate transparent adversarial patches \mathcal{P}^{adv} for target objects in the scene to make these objects undetectable and cause navigation failure. The problem is formulated as finding the optimal texture that maximizes the adversarial loss

$$\max_{\mathcal{P}^{adv}} \left\{ \mathbb{E}_{\mathbf{v} \in V} \mathcal{L}_{attack}[f(\mathcal{R}(\mathcal{S}, \mathcal{P}^{adv}; L, \mathbf{v})), y] \right\}, \quad (1)$$

where $\hat{o} = \mathcal{R}(\mathcal{S}, \mathcal{P}^{adv}; L, \mathbf{v})$ represents the rendered image, L denotes lighting conditions, and \mathbf{v} is the viewpoint from distribution V . \mathcal{L}_{attack} is the loss that induces detection errors in the navigation model. The challenge lies in ensuring adversarial robustness across multiple viewpoints. Further details are provided in Sec. III-C and Sec. III-D.

C. Object-aware Sampling

Since target object visibility varies with angles, distances, and scene contexts, we employ a specialized sampling strategy to obtain the most valuable viewpoints for optimizing the patch. We randomly initialize camera viewpoints and filter configurations based on the navigation model’s detection confidence, yielding a distribution V that is optimal for optimization. Cameras are positioned around the target

object, and the viewpoint distribution is defined as:

$$\begin{aligned} V &= \{(\mathbf{p}_i(r), \phi_i) \mid r \in R, \sigma(f(o) = 1)\}, \\ i &\in \{0, 1, \dots, N-1\}, \\ \mathbf{p}_i(r) &= \left(c_x + r \cos\left(\frac{2\pi i}{N}\right), c_y, c_z + r \sin\left(\frac{2\pi i}{N}\right) \right), \\ \phi_i &= \left(0, \frac{2\pi i}{N} - \frac{\pi}{2}, \pi \right). \end{aligned} \quad (2)$$

Here, $\mathbf{p}_i(r)$ represents the camera position around the object center (c_x, c_y, c_z) , with radii $r \in R$ ensuring layered coverage. ϕ_i denotes the camera orientation, and N is the number of cameras per circle. The indicator function $\sigma(x) = 1_{x \geq \tau}$ filters configurations based on detection confidence.

D. Multi-view Optimization

To address the challenge of the patch’s multi-view effectiveness, we optimize the patch using a physics-based differentiable renderer and the sampled viewpoint distribution. First-person images from these viewpoints are rendered and fed into the navigation model to compute the total detection loss. Gradients from multiple views are used to optimize the patch texture with a gradient-based method. The rendering process is defined as:

$$o = \mathcal{R}(\mathcal{S}; L, \mathbf{p}_i(r), \phi_i), \quad (3)$$

$$\hat{o} = \mathcal{R}(\mathcal{S}, \mathcal{P}^{adv}; L, \mathbf{p}_i(r), \phi_i), \quad (4)$$

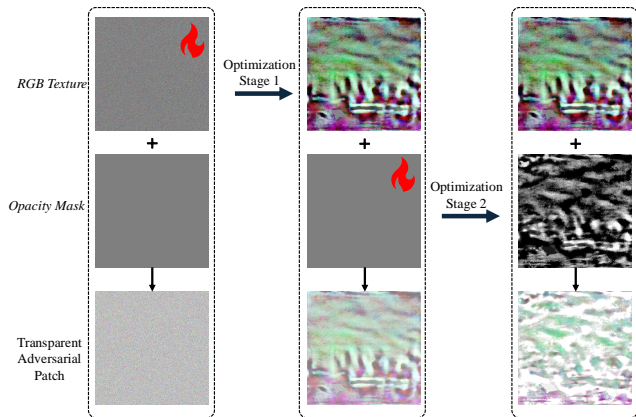


Fig. 3. **Opacity Optimization Strategy.** The first stage optimizes the RGB texture to enhance the attack’s efficacy, while the second stage refines the opacity mask to reduce the patch’s detectability to the human eye.

where o and \hat{o} are images without and with the adversarial patch, respectively. The final gradient-based update for the patch texture is:

$$\mathcal{P}_{\text{adv}} = \mathcal{P}_{\text{adv}} + \alpha \cdot \text{sign}(\nabla_{\mathcal{P}_{\text{adv}}} L_{\text{total}}(f(\mathcal{R}(\mathcal{S}_{\text{adv}}, c)), y)), \quad (5)$$

where α is the learning rate, and $\nabla_{\mathcal{P}_{\text{adv}}} L_{\text{total}}$ is the gradient of the total loss with respect to the patch texture. This iterative process ensures robust adversarial patches across multiple viewpoints and lighting conditions.

E. Opacity Optimization

To improve the naturalness of the patch, we incorporate an opacity optimization mechanism. Digitally, our adversarial patch consists of a base texture image with three RGB color channels and a single-channel opacity mask, where transparency values range from 0 to 255, with 255 representing full opacity and 0 representing full transparency. Both the base texture and the opacity mask are optimized for effectiveness. Intuitively, we consider the primary role of the texture to be enhancing the attack’s efficacy, while the opacity mainly serves to reduce the patch’s visibility to the human eye. Thus, as shown in Fig. 3, we employ a two-stage optimization strategy. In the first stage, we randomly initialize a three-channel RGB texture and a constant single-channel opacity mask, combining them to form the initial adversarial patch. This patch is iteratively optimized using the strategies described in Section III-C and Section III-D, resulting in an effective adversarial texture. In the second stage, we optimize the opacity mask based on the optimized texture, using the same optimization approach. We hypothesize that optimizing the opacity mask enhances the texture variation across different regions of the patch, making it less detectable to human observers. All optimizations are conducted using a gradient-based PGD (Projected Gradient Descent) method.

Physically, this transparency image can be printed on transparent paper using a laser printer and then directly affixed to the target object. This approach is particularly practical in navigation scenarios, as it eliminates the need

TABLE I
ATTACK PERFORMANCE ON MULTI-VIEW OBJECT DETECTION.

Attack Method	ASR↑(%)
No Attack	19.01
Camouflage [2]	85.12(66.11↑)
Adversarial Patch (Random Texture)	29.75(10.74↑)
Adversarial Patch (2D Optimized Texture)	74.38(55.37↑)
<i>Ours</i> Patch (Multi-view Optimized Texture)	89.26 (70.25↑)
<i>Ours</i> Patch (Multi-view Optimized Texture & Opacity)	98.35 (79.34↑)

TABLE II
ATTACK PERFORMANCE ON THE HM3D SCENE DATASET FOR NAVIGATION.

Attack Method	SR↓(%)	SPL↓(%)	DTS↑(m)
No Attack	19.01	63.03	0.04
Camouflage [2]	100.00(0.00↓)	56.37(6.66↓)	0.04(0.00↑)
<i>Ours</i> Patch	60.00 (40.00↓)	14.81 (48.22↓)	1.68 (1.64↑)

to modify the properties of existing scene objects. Moreover, the patch’s adjustable transparency ensures it remains inconspicuous to human observers.

IV. EXPERIMENTS

A. Experimental Setup

Settings. We use the modular-based navigation agent from [22] for ObjectNav, which includes a Mask R-CNN [44] for object instance segmentation, predicting 9 target categories from HM3D images. Our setup follows the 2022 Habitat ObjectNav Challenge [45]. The adversarial patch is 512×512 , initialized with Gaussian noise, and randomly placed on the target. Mitsuba 3 [46] serves as the renderer, with planar area lights or “constant” scene lighting at intensity 40, and a camera resolution of 512×512 . The detection confidence threshold is 0.5. We apply PGD (L2/Linf) attacks with a maximum perturbation of 5 units over 100 steps, with a learning rate of 1.

Datasets. We conduct adversarial attack experiments on ObjectNav and the HM3D dataset [47] using the Habitat simulator [48], [20]. The TV monitor is chosen as the attack target, with one scene from the validation dataset used for white-box optimization, targeting a 512×512 transparent patch.

Evaluations. We evaluate attack performance using three metrics from [22]: Success Rate (SR), Success weighted by Path Length (SPL), and Distance to Goal (DTS). SR measures the agent’s ability to successfully locate the target object, while SPL considers both the success rate and the efficiency of the path taken. DTS quantifies the remaining distance between the agent and the goal at the end of each episode. Additionally, we measure the Attack Success Rate (ASR) for multi-view object detection in the scene.

B. Attack Performance

Table I presents the Attack Success Rate (ASR) for multi-view target detection in a navigation scenario, where 121 viewpoints surrounding the target were sampled using our



Fig. 4. Visualization of the attack performance of our adversarial patch compared to 3D camouflage in the navigation task. The first row shows the adversarial scenario with 3D camouflage, where the agent was still able to successfully navigate and locate the target. In contrast, in the scenario with our adversarial patch, the agent failed to detect the target even after 499 steps, resulting in navigation failure. This highlights the superior attack performance of our method compared to the baseline 3D camouflage approach.



Fig. 5. Visualization of adversarial patches under different ablation conditions. We display six viewpoints from left to right. From top to bottom, "Random Noise" applies random textures without opacity, making the patch more visible in the scene. "Optimized Texture" refines the texture through multi-view optimization, significantly altering the texture. "Optimized Opacity" further optimizes the opacity, "No Attack" represents the original clean scene. It is evident that after applying opacity optimization, the Natural of the patch improves significantly, aligning with the goals of physical adversarial attacks: effective performance, easy implementation, and reduced visibility to the human eye.

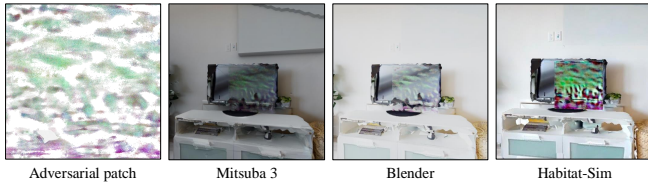


Fig. 6. **Visualization of adversarial patches with opacity under different renderers.** Due to differences in physical rendering techniques and lighting setups, this highlights the challenge of ensuring cross-renderer transferability and maintaining attack effectiveness. Notably, the habitat-sim renderer lacks support for transparent materials, making the texture appear more visible in its renderings.

object-aware sampling strategy. We compared our method with previous physically realizable approaches, specifically the camouflage adversarial patch method. The camouflage approach is based on [2], where we focused on the Spatially Contextual Perturbations module and incorporated multi-view optimization, as the Temporal Attention Stimulus module is not applicable to navigation tasks. The adversarial patch [3], [4], [5], [6], [7], [8], [9], [10], [11] was compared using random textures and 2D-optimized textures without differentiable rendering and multi-view optimization. Since direct placement of the patch on the target can be too conspicuous, we set the opacity to 0.8. Our experiments show that the proposed multi-view sampling strategy increased ASR by up to 70.25%. With the addition of opacity optimization, ASR further improved, reaching up to 79.24%, surpassing the baseline performance.

Table II shows the attack performance of our adversarial patch, which underwent multi-view optimization and opacity optimization, in the navigation task. Since camouflage [2] is the only method targeting embodied navigation, we limited our comparison to it. Our method reduced the navigation success rate by approximately 40% in the surrogate scene. The visualization and qualitative analysis in Fig. 4 further illustrate the patch’s effectiveness, where the agent failed to detect the target even after 499 steps, resulting in navigation failure. This demonstrates superior attack performance compared to the baseline 3D camouflage method.

C. Ablation Study

In this section, we conduct ablation experiments to investigate the impact of two components: the multi-view optimization strategy based on object-aware sampling and the opacity optimization strategy. The objective is to provide insights into the key factors driving performance improvements.

Effect of multi-view optimization based on object-aware sampling. The experimental results are shown in Table III. As observed, when neither multi-view texture optimization nor opacity optimization is applied, the ASR is the lowest at 28.93%. When only single-view texture optimization is applied, there is an improvement, and multi-view texture optimization leads to even higher performance. When both texture and opacity are optimized, the ASR reaches its highest value of 99.17%, validating the effectiveness of our multi-view optimization strategy. The visualizations are presented in Fig. 5, where we display six viewpoints from

TABLE III
ABLATION STUDY ON ATTACK COMPONENTS.

Texture Optimization	Opacity Optimization	Viewpoints	ASR↑(%)
✗	✗	-	28.93
✓	✗	1	73.55(44.62↑)
✓	✗	121	89.26(60.33↑)
✓	✓	121	99.17(70.24↑)

TABLE IV
ABLATION STUDY ON OPACITY VALUE.

Method	Opacity Value(%)	ASR↑(%)
Texture Random	0.20	24.79
	0.40	21.49
	0.60	15.70
	0.80	29.75
Texture Optimized	0.20	22.31
	0.40	71.90
	0.60	90.91
	0.80	87.60

left to right. From top to bottom, we show the random texture, optimized texture, optimized opacity, and the original scene, respectively. It is evident that after applying opacity optimization, the visual quality of the patch improves significantly, aligning with the goals of physical adversarial attacks: easy to implement, effective performance, and less visible to the human eye.

Effect of opacity value. In addition, we studied the effect of different opacity levels in Table IV. We applied varying levels of opacity to both random and optimized textures. At an opacity of 0.2, the patch is almost completely transparent and nearly invisible to the human eye, while at 0.8, it is nearly fully opaque. The higher the opacity, the higher the ASR, but the patch becomes more noticeable. Therefore, we selected an initial opacity of 0.6 for both texture and opacity optimization in our quantitative experiments, as it provides a balance between attack effectiveness and visibility. Finally, in Fig. 6, we present the rendered effects of the adversarial patch with different opacity values under various renderers.

V. CONCLUSION

In this paper, we address the challenge of adversarial robustness in embodied navigation tasks and the physical feasibility of attack methods. We propose a practical attack method for embodied navigation by attaching adversarial patches with learnable textures and opacity to objects. Specifically, to ensure effectiveness across varying viewpoints, we employ a multi-view optimization strategy based on object-aware sampling, which uses feedback from the navigation model to optimize the patch’s texture. To make the patch inconspicuous to human observers, we introduce a two-stage opacity optimization mechanism, where opacity is refined after texture optimization. Experimental results show our adversarial patches reduce navigation success rates by about 40%, outperforming previous methods in practicality, effectiveness, and naturalness.

REFERENCES

- [1] C. Ying, Y. Qiaoben, X. Zhou, H. Su, W. Ding, and J. Ai, "Consistent attack: Universal adversarial perturbation on embodied vision navigation," *Pattern Recognition Letters*, vol. 168, pp. 57–63, 2023.
- [2] A. Liu, T. Huang, X. Liu, Y. Xu, Y. Ma, X. Chen, S. J. Maybank, and D. Tao, "Spatiotemporal attacks for embodied agents," in *Computer Vision—ECCV 2020: 16th European Conference, Glasgow, UK, August 23–28, 2020, Proceedings, Part XVII 16*. Springer, 2020, pp. 122–138.
- [3] T. B. Brown, D. Mané, A. Roy, M. Abadi, and J. Gilmer, "Adversarial patch," *arXiv preprint arXiv:1712.09665*, 2017.
- [4] K. Eykholt, I. Evtimov, E. Fernandes, B. Li, A. Rahmati, C. Xiao, A. Prakash, T. Kohno, and D. Song, "Robust physical-world attacks on deep learning visual classification," in *Proceedings of the IEEE conference on computer vision and pattern recognition*, 2018, pp. 1625–1634.
- [5] N. Akhtar, A. Mian, N. Kardan, and M. Shah, "Advances in adversarial attacks and defenses in computer vision: A survey," *IEEE Access*, vol. 9, pp. 155 161–155 196, 2021.
- [6] C. Yang, A. Kortylewski, C. Xie, Y. Cao, and A. Yuille, "Patchattack: A black-box texture-based attack with reinforcement learning," in *European Conference on Computer Vision*. Springer, 2020, pp. 681–698.
- [7] X. Liu, H. Yang, Z. Liu, L. Song, H. Li, and Y. Chen, "Dpatch: An adversarial patch attack on object detectors," *arXiv preprint arXiv:1806.02299*, 2018.
- [8] X. Yang, Y. Dong, T. Pang, Z. Xiao, H. Su, and J. Zhu, "Controlable evaluation and generation of physical adversarial patch on face recognition," *arXiv preprint arXiv:2203.04623*, 2022.
- [9] X. Wei, S. Ruan, Y. Dong, and H. Su, "Distributional modeling for location-aware adversarial patches," *arXiv preprint arXiv:2306.16131*, 2023.
- [10] C. Kang, Y. Dong, Z. Wang, S. Ruan, Y. Chen, H. Su, and X. Wei, "Diffender: Diffusion-based adversarial defense against patch attacks."
- [11] Z. Xiao, X. Gao, C. Fu, Y. Dong, W. Gao, X. Zhang, J. Zhou, and J. Zhu, "Improving transferability of adversarial patches on face recognition with generative models," in *Proceedings of the IEEE/CVF conference on computer vision and pattern recognition*, 2021, pp. 11 845–11 854.
- [12] S. Oslund, C. Washington, A. So, T. Chen, and H. Ji, "Multiview robust adversarial stickers for arbitrary objects in the physical world," *Journal of Computational and Cognitive Engineering*, vol. 1, no. 4, pp. 152–158, 2022.
- [13] Z. Hu, W. Chu, X. Zhu, H. Zhang, B. Zhang, and X. Hu, "Physically realizable natural-looking clothing textures evade person detectors via 3d modeling," in *Proceedings of the IEEE/CVF Conference on Computer Vision and Pattern Recognition*, 2023, pp. 16 975–16 984.
- [14] H. Wang, W. Liang, L. V. Gool, and W. Wang, "Towards versatile embodied navigation," *Advances in neural information processing systems*, vol. 35, pp. 36 858–36 874, 2022.
- [15] D. S. Chaplot, D. P. Gandhi, A. Gupta, and R. R. Salakhutdinov, "Object goal navigation using goal-oriented semantic exploration," *Advances in Neural Information Processing Systems*, vol. 33, pp. 4247–4258, 2020.
- [16] T. Gervet, S. Chintala, D. Batra, J. Malik, and D. S. Chaplot, "Navigating to objects in the real world," *Science Robotics*, vol. 8, no. 79, p. eadf6991, 2023.
- [17] P. Chattopadhyay, J. Hoffman, R. Mottaghi, and A. Kembhavi, "Robustnav: Towards benchmarking robustness in embodied navigation," in *Proceedings of the IEEE/CVF International Conference on Computer Vision*, 2021, pp. 15 691–15 700.
- [18] P. Anderson, A. Chang, D. S. Chaplot, A. Dosovitskiy, S. Gupta, V. Koltun, J. Kosecka, J. Malik, R. Mottaghi, M. Savva *et al.*, "On evaluation of embodied navigation agents," *arXiv preprint arXiv:1807.06757*, 2018.
- [19] F. Zhu, Y. Zhu, V. Lee, X. Liang, and X. Chang, "Deep learning for embodied vision navigation: A survey," *arXiv preprint arXiv:2108.04097*, 2021.
- [20] A. Szot, A. Clegg, E. Undersander, E. Wijmans, Y. Zhao, J. Turner, N. Maestre, M. Mukadam, D. Chaplot, O. Maksymets, A. Gokaslan, V. Vondrus, S. Dharur, F. Meier, W. Galuba, A. Chang, Z. Kira, V. Koltun, J. Malik, M. Savva, and D. Batra, "Habitat 2.0: Training home assistants to rearrange their habitat," in *Advances in Neural Information Processing Systems (NeurIPS)*, 2021.
- [21] M. Savva, A. Kadian, O. Maksymets, Y. Zhao, E. Wijmans, B. Jain, J. Straub, J. Liu, V. Koltun, J. Malik *et al.*, "Habitat: A platform for embodied ai research," in *Proceedings of the IEEE/CVF international conference on computer vision*, 2019, pp. 9339–9347.
- [22] A. J. Zhai and S. Wang, "Peanut: predicting and navigating to unseen targets," in *Proceedings of the IEEE/CVF International Conference on Computer Vision*, 2023, pp. 10926–10935.
- [23] I. J. Goodfellow, J. Shlens, and C. Szegedy, "Explaining and harnessing adversarial examples," *arXiv preprint arXiv:1412.6572*, 2014.
- [24] N. Carlini and D. Wagner, "Towards evaluating the robustness of neural networks," in *2017 IEEE Symposium on Security and Privacy (SP)*. Ieee, 2017, pp. 39–57.
- [25] C. Xiao, B. Li, J.-Y. Zhu, W. He, M. Liu, and D. Song, "Generating adversarial examples with adversarial networks," *arXiv preprint arXiv:1801.02610*, 2018.
- [26] Y. Huang, Y. Dong, S. Ruan, X. Yang, H. Su, and X. Wei, "Towards transferable targeted 3d adversarial attack in the physical world," in *Proceedings of the IEEE/CVF Conference on Computer Vision and Pattern Recognition*, 2024, pp. 24 512–24 522.
- [27] N. Suryanto, Y. Kim, H. T. Larasati, H. Kang, T.-T.-H. Le, Y. Hong, H. Yang, S.-Y. Oh, and H. Kim, "Active: Towards highly transferable 3d physical camouflage for universal and robust vehicle evasion," in *Proceedings of the IEEE/CVF International Conference on Computer Vision*, 2023, pp. 4305–4314.
- [28] N. Suryanto, Y. Kim, H. Kang, H. T. Larasati, Y. Yun, T.-T.-H. Le, H. Yang, S.-Y. Oh, and H. Kim, "Dta: Physical camouflage attacks using differentiable transformation network," in *Proceedings of the IEEE/CVF Conference on Computer Vision and Pattern Recognition*, 2022, pp. 15 305–15 314.
- [29] D. Wang, T. Jiang, J. Sun, W. Zhou, Z. Gong, X. Zhang, W. Yao, and X. Chen, "Fca: Learning a 3d full-coverage vehicle camouflage for multi-view physical adversarial attack," in *Proceedings of the AAAI conference on artificial intelligence*, vol. 36, no. 2, 2022, pp. 2414–2422.
- [30] J. Wang, A. Liu, Z. Yin, S. Liu, S. Tang, and X. Liu, "Dual attention suppression attack: Generate adversarial camouflage in physical world," in *Proceedings of the IEEE/CVF conference on computer vision and pattern recognition*, 2021, pp. 8565–8574.
- [31] X. Wei, Y. Guo, J. Yu, and B. Zhang, "Simultaneously optimizing perturbations and positions for black-box adversarial patch attacks," *IEEE transactions on pattern analysis and machine intelligence*, 2022.
- [32] M. Sharif, S. Bhagavatula, L. Bauer, and M. K. Reiter, "Accessorize to a crime: Real and stealthy attacks on state-of-the-art face recognition," in *Proceedings of the 2016 ACM SIGSAC conference on computer and communications security*, 2016, pp. 1528–1540.
- [33] A. Athalye, L. Engstrom, A. Ilyas, and K. Kwok, "Synthesizing robust adversarial examples," in *International conference on machine learning*. PMLR, 2018, pp. 284–293.
- [34] R. R. Wiyatno and A. Xu, "Physical adversarial textures that fool visual object tracking," in *Proceedings of the IEEE/CVF International Conference on Computer Vision*, 2019, pp. 4822–4831.
- [35] A. Pal, Y. Qiu, and H. Christensen, "Learning hierarchical relationships for object-goal navigation," in *Conference on Robot Learning*. PMLR, 2021, pp. 517–528.
- [36] H. Du, X. Yu, and L. Zheng, "Vtnet: Visual transformer network for object goal navigation," *arXiv preprint arXiv:2105.09447*, 2021.
- [37] N. Kim, O. Kwon, H. Yoo, Y. Choi, J. Park, and S. Oh, "Topological semantic graph memory for image-goal navigation," in *Conference on Robot Learning*. PMLR, 2023, pp. 393–402.
- [38] L. Mezghan, S. Sukhbaatar, T. Lavril, O. Maksymets, D. Batra, P. Bojanowski, and K. Alahari, "Memory-augmented reinforcement learning for image-goal navigation," in *2022 IEEE/RSJ International Conference on Intelligent Robots and Systems (IROS)*. IEEE, 2022, pp. 3316–3323.
- [39] A. Majumdar, G. Aggarwal, B. Devnani, J. Hoffman, and D. Batra, "Zson: Zero-shot object-goal navigation using multimodal goal embeddings," *Advances in Neural Information Processing Systems*, vol. 35, pp. 32 340–32 352, 2022.
- [40] S.-M. Park and Y.-G. Kim, "Visual language navigation: A survey and open challenges," *Artificial Intelligence Review*, vol. 56, no. 1, pp. 365–427, 2023.
- [41] Y. Qi, Z. Pan, S. Zhang, A. van den Hengel, and Q. Wu, "Object-and-action aware model for visual language navigation," in *European Conference on Computer Vision*. Springer, 2020, pp. 303–317.

- [42] C. Huang, O. Mees, A. Zeng, and W. Burgard, "Visual language maps for robot navigation," in *2023 IEEE International Conference on Robotics and Automation (ICRA)*. IEEE, 2023, pp. 10 608–10 615.
- [43] A. Das, S. Datta, G. Gkioxari, S. Lee, D. Parikh, and D. Batra, "Embodied question answering," in *Proceedings of the IEEE conference on computer vision and pattern recognition*, 2018, pp. 1–10.
- [44] K. He, G. Gkioxari, P. Dollár, and R. Girshick, "Mask r-cnn," in *Proceedings of the IEEE international conference on computer vision*, 2017, pp. 2961–2969.
- [45] K. Yadav, J. Krantz, R. Ramrakhya, S. K. Ramakrishnan, J. Yang, A. Wang, J. Turner, A. Gokaslan, V.-P. Berges, R. Mottaghi, O. Maksymets, A. X. Chang, M. Savva, A. Clegg, D. S. Chaplot, and D. Batra, "Habitat challenge 2023," <https://aihabitat.org/challenge/2023/>, 2023.
- [46] W. Jakob, S. Speierer, N. Roussel, and D. Vicini, "Dr.jit: A just-in-time compiler for differentiable rendering," *Transactions on Graphics (Proceedings of SIGGRAPH)*, vol. 41, no. 4, Jul. 2022.
- [47] S. K. Ramakrishnan, A. Gokaslan, E. Wijmans, O. Maksymets, A. Clegg, J. M. Turner, E. Undersander, W. Galuba, A. Westbury, A. X. Chang, M. Savva, Y. Zhao, and D. Batra, "Habitat-matterport 3d dataset (HM3d): 1000 large-scale 3d environments for embodied AI," in *Thirty-fifth Conference on Neural Information Processing Systems Datasets and Benchmarks Track*, 2021. [Online]. Available: <https://arxiv.org/abs/2109.08238>
- [48] M. Savva, A. Kadian, O. Maksymets, Y. Zhao, E. Wijmans, B. Jain, J. Straub, J. Liu, V. Koltun, J. Malik, D. Parikh, and D. Batra, "Habitat: A Platform for Embodied AI Research," in *Proceedings of the IEEE/CVF International Conference on Computer Vision (ICCV)*, 2019.